Optimal Operation of a Josephson Parametric Amplifier for Vacuum Squeezing

M. Malnou,[1,2,*] D. A. Palken,[1,2] Leila R. Vale,[3] Gene C. Hilton,[3] and K. W. Lehnert[1,2]

[1]*JILA, National Institute of Standards and Technology and the University of Colorado, Boulder, Colorado 80309, USA*

[2]*Department of Physics, University of Colorado, Boulder, Colorado 80309, USA*

[3]*National Institute of Standards and Technology, Boulder, Colorado 80305, USA*

(Received 7 November 2017; revised manuscript received 10 January 2018; published 17 April 2018)

A Josephson parametric amplifier (JPA) can create squeezed states of microwave light, lowering the noise associated with certain quantum measurements. We experimentally study how the JPA's pump influences the phase-sensitive amplification and deamplification of a coherent tone's amplitude when that amplitude is commensurate with vacuum fluctuations. We predict and demonstrate that, by operating the JPA with a single current pump whose power is greater than the value that maximizes gain, the amplifier distortion is reduced and, consequently, squeezing is improved. Optimizing the singly pumped JPA's operation in this fashion, we directly observe 3.87 ± 0.03 dB of vacuum squeezing over a bandwidth of 30 MHz.

DOI: 10.1103/PhysRevApplied.9.044023

I. INTRODUCTION

Josephson parametric amplifiers (JPAs) have enabled many advances in quantum-information measurements, such as the observation of quantum jumps [1–3], fast qubit initialization [4], and characterization of microwave single-photon sources [5]. When operated in a phase-sensitive mode, a JPA amplifies one quadrature of the electromagnetic field while deamplifying the other, enabling the squeezing of vacuum states below the standard quantum limit. Such squeezed states can improve qubit readout fidelity in dispersive measurements [6–9], help to better measure the motion of a mechanical oscillator [10], and enhance the signal-to-noise ratio of spin-echo detection in a magnetic resonance experiment [11]. Similarly, they could accelerate haloscope-based searches [12] for axionic dark matter [13], an application in which JPAs have already been successfully deployed, albeit only in a phase-insensitive mode of operation [14,15].

In principle, a JPA can squeeze one quadrature of vacuum while amplifying the other by the same amount [16–18]. However, in practice, vacuum squeezing is limited by microwave losses and distortion due to amplifier saturation [19,20]. Minimizing loss through improved, low-loss elements or via fewer microwave connections remains an important challenge, and, to that end, on-chip circulators [21–25], flux-pumped parametric amplifiers [26–29], and directional amplifiers [21,30] are promising. We here address the other challenge: distortion.

A JPA is essentially a nonlinear LC resonator whose nonlinearity comes from the Josephson junctions comprising its inductance [16,31]. Parametric oscillation of the circuit converts a pair of pump photons at angular frequency ω_p into a signal photon at ω_s and a complementary idler photon at ω_i in a four-wave process: $2\omega_p = \omega_s + \omega_i$. In the degenerate case, the pump is centered about the amplification band and $\omega_p \simeq \omega_s \simeq \omega_i$.

Different combinations of pump power and frequency will produce the same gain, and one typically operates at points first-order-insensitive to pump power fluctuations, i.e., on the line of maximum gain (LMG) [32]. Here a JPA can achieve more than 20 dB of gain and maintain a linear relationship between the input- and output-signal powers. Squeezing, however, is more susceptible to nonlinearities that distort the output, arising when signal photons in the resonator greatly affect the pump's amplitude. These nonlinear effects impact the squeezed quadrature at gains much lower than those where they affect the amplified quadrature. Pump stiffness can nonetheless be improved by double pumping [33] or flux pumping [26–29], at the cost of increased design and control complexity.

In this article, we demonstrate how a single-pumped JPA can be optimized for squeezing. We show that pumping it with a power greater than that which maximizes gain at a given pump frequency improves pump stiffness and minimizes signal distortion. We first experimentally study this effect on a coherent tone whose power is comparable to vacuum and measure how it is transformed by a JPA operated at constant gain for various pump powers and frequencies. Then, we determine an optimal operating point for which the distortion is minimized. Finally, we use a

*maxime.malnou@colorado.edu

 © 2018 American Physical Society

second JPA as a phase-sensitive preamplifier to measure a vacuum squeezed state prepared by the first JPA and show that squeezing follows the same dependence on the operating point. With optimized pump power and frequency, and while keeping microwave losses low, we generate, transport, and read out a state 3.87 ± 0.03 dB below vacuum. This could more than double the speed at which the search for axionic dark matter is carried out [13].

II. SIGNAL TRANSFORMATION IN PHASE SPACE

In the JPAs we study, the inductance L is implemented with a series array of N_s balanced dc superconducting quantum interference devices (SQUIDs). When shunted by a capacitor C, it forms a nonlinear resonant circuit whose frequency is tunable with magnetic flux applied through the SQUID loops. Such a tunable Kerr circuit (TKC) is described to leading nonlinear order by the Hamiltonian

$$\hat{H} = \hbar\omega_0 \hat{n} + \frac{\hbar K}{2}\hat{n}^2, \tag{1}$$

which gives rise to a Duffing oscillator equation of motion [32]. Here $\hat{n} = \hat{a}^\dagger \hat{a}$ gives the number of photons in the cavity, $K = (-\hbar\omega_0^2/16 N_s \phi_0 I_c)$ is the Kerr nonlinearity, I_c is the critical current of each junction, $\omega_0 = 1/\sqrt{LC}$ is the TKC's bare resonance angular frequency, and ϕ_0 is the reduced magnetic flux quantum.

When coupled to an external port at field-decay rate γ, a classical limit of the input-output theory [34,35] determines the complex field amplitude, or phasor, at the output b_{out} from the incoming field amplitude b_{in} as

$$b_{\text{out}} = b_{\text{in}}\left(1 - \frac{2\gamma}{i(\Delta + Kn) + \gamma}\right). \tag{2}$$

Here, $n = \langle \hat{n} \rangle$ is the average photon number and $\Delta = \omega_0 - \omega_p$ is the detuning between the bare resonant angular frequency and the input phasor's angular frequency. This semiclassical model does not properly treat the quantum noise at the JPA's input, but it nonetheless makes useful predictions of its behavior on a qualitative level. While beyond the scope of this article, an analytic treatment of a fully quantum parametric oscillator can be found in Ref. [36].

A JPA is often approximated as amplifying an infinitesimally weak signal $b_{s,\text{in}} e^{i\theta}$ in the presence of a large pump tone $b_{p,\text{in}}$ (taken as a phase reference), such that $b_{\text{in}} = b_{p,\text{in}} + b_{s,\text{in}} e^{i\theta}$. However, Eq. (2) remains valid without the stiff pump approximation, providing a mapping between the input and output within the bandwidth of the lossless JPA. This transformation being unitary below bifurcation, the gain derives from the sharp dependence of the output phase on the input amplitude. The photon number n is determined by the cubic equation [35]

$$n^3 + \frac{2\Delta}{K} n^2 + \frac{\Delta^2 + \gamma^2}{K^2} n = \frac{2\gamma}{K^2} |b_{\text{in}}|^2. \tag{3}$$

Figure 1(a) shows how a family of real input pump tones with varying amplitude $b_{p,\text{in}}$ maps onto complex outputs $b_{p,\text{out}}$. They are calculated from Eqs. (2) and (3), with Δ constant. A particular input phasor and its corresponding output are indicated with black arrows, illustrating the JPA's behavior at the greatest phase sensitivity, i.e., at maximum gain.

When adding a signal $b_{s,\text{in}} e^{i\theta}$, the total input phasor b_{in} undergoes a θ-dependent transformation. One quadrature of the output signal $b_{s,\text{out}}$ is amplified, while the orthogonal one is deamplified. At low JPA gain or infinitesimal input signal, $b_{s,\text{out}}$ exhibits an elliptic shape. However, as the

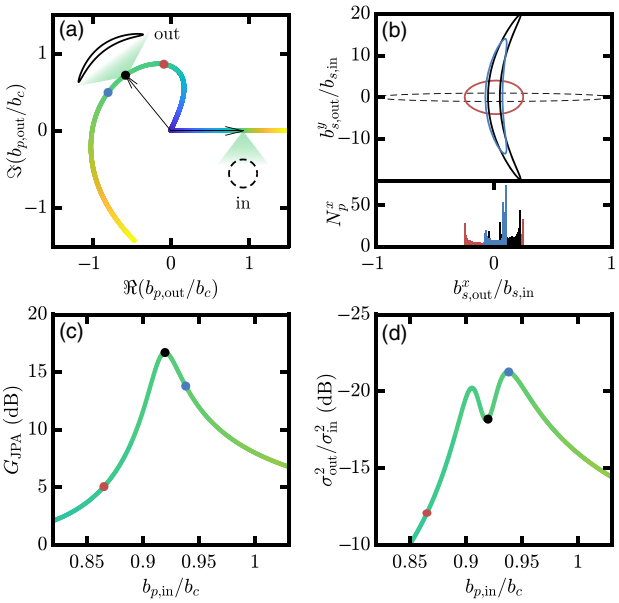

FIG. 1. Theory of distortion in a JPA. Calculations for $\gamma = 2\pi \times 54.5$ MHz, $\Delta/\gamma = 1.54$, $K/\gamma = -8.3 \times 10^{-4}$, and a quality factor $Q = \omega_0/2\gamma = 65$, typical values for our array-based JPAs. (a) A family of input pump phasors of different amplitudes describes the horizontal, colored line. These inputs map onto output phasors distributed along the correspondingly colored curve in the complex plane. They are normalized by the critical amplitude $b_c = \sqrt{(4\gamma^2/3|K|\sqrt{3})}$. Two black arrows indicate the pair of input and output phasors at maximum gain. At this operating point, an enlargement shows how an input-signal phasor $b_{s,\text{in}} e^{i\theta}$ maps onto a banana at the output. Two other operating points (red and blue) are indicated. (b) The input phasor, simulated with 360 different θ angles (dashed circle, deformed due to the unequal axis scaling), is processed by the JPA for three different pump powers corresponding to the operating points from (a). The lower panel shows the distribution of points N_p^x of these phasors, when projected onto the deamplified x axis. The JPA direct gain (c) and the deamplified quadrature variance (d) are plotted as a function of the pump amplitude.

input signal or gain increases, it distorts into a "banana," indicating that the pump is no longer stiff. Figure 1(b) represents such distortions, or deviations from the elliptical output of an ideal degenerate parametric amplifier [11,19], at three different JPA gains obtained by varying the pump's amplitude, for a probe tone whose power is equivalent to half a photon over the JPA's bandwidth. They are rotated to share their amplified and deamplified quadratures, respectively, $b^y_{s,\mathrm{out}}$ and $b^x_{s,\mathrm{out}}$. At the point of maximum gain, $b_{s,\mathrm{out}}$ actually has a larger projection on the deamplified axis x than at intermediate gain, where the projection onto this axis is minimal. When a signal is detuned from the pump, it creates output rotating phasors such as these, and the direct, or signal power, gain is expressed as [37]

$$G = \frac{\langle G_\theta \rangle + 1}{2}, \tag{4}$$

with $\langle G_\theta \rangle$ the average ratio of output to input rotating phasor power. Figure 1(c) shows the JPA direct gain as a function of pump amplitude $b_{p,\mathrm{in}}$.

A vacuum state, considered semiclassically as a statistical ensemble of phasors, should undergo a similar distortion when squeezed by a JPA. This effect degrades the maximal achievable squeezing, because it increases the noise variance along the deamplified quadrature axis. To make a qualitative estimate of the attainable degree of squeezing, we first project the distributions of input and output points onto the deamplified quadrature axis [Fig. 1(b)] and then compare the variances, (σ^2_{in}) and $(\sigma^2_{\mathrm{out}})$, of these projections. Figure 1(d) shows the ratio $\sigma^2_{\mathrm{out}}/\sigma^2_{\mathrm{in}}$, as a function of the pump power, for a given pump frequency. Deamplification is maximized when this ratio is minimized. Strikingly, the pump amplitude that produces maximum gain fails to yield maximum deamplification due to phasor distortion of the vacuum-sized input. Instead, deamplification reaches a global maximum at an amplitude greater than that at maximum gain, i.e., above the LMG, where phasor distortion is better mitigated. We demonstrate this behavior in Sec. III, enabling the optimization of vacuum squeezing discussed in Sec. IV.

III. DEAMPLIFICATION OF A COHERENT TONE

In a first experiment, we investigate the distortion of a vacuum-sized coherent tone when varying the JPA operating point, by changing the pump power and frequency. A single cryogenic experimental setup is used for studying distortion and vacuum squeezing, discussed in Sec. IV. It comprises two identical JPAs (Appendix A) connected to each other, as shown in Fig. 2. The first we label the squeezer (SQ) and the second the amplifier (AMP). Each can be independently tuned via its own superconducting coil, and a variable-temperature stage (VTS) is used to inject known thermal noise into the amplifier chain and measure the SQ added noise (Appendix C). We use

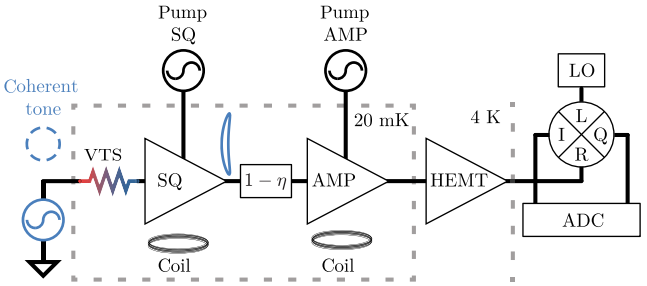

FIG. 2. Experimental setup for coherent tone distortion and vacuum squeezing. The SQ and AMP are mounted in series. When studying distortion, the AMP is detuned and not pumped, while a microwave generator sends a known coherent tone at the chain's input (dashed circle), then processed by the SQ. Microwave losses between the SQ and AMP are parametrized by η. After subsequent amplification by a cryogenic high-electron mobility transistor (HEMT), the tone is mapped to a low frequency using an in-phase/quadrature (IQ) mixer and a local oscillator (LO). An analog-to-digital converter (ADC) records the output signal's I and Q quadratures.

microwave generators to pump the two JPAs and send coherent tones to the input of the chain. An IQ mixer demodulates the output quadratures with respect to a local oscillator (LO). In this first experiment, we do not use the AMP; by tuning it more than 1 GHz below the SQ band, it acts as a passive element of unit gain.

In order to compare the distortion and SQ direct gain G_S at particular operating points, we find G_S (measured with a vector network analyzer; see Appendix A) as a function of pump power P_p and frequency f_p. We identify a critical point at which the gain diverges and describe the pump power and frequency as fractions of these critical values [Fig. 3(a)]. The dashed black line shows the LMG. We compare deamplification when operating the SQ at points with equal gains below, above, and on this line. From the weaker dependence of gain on the incident power above

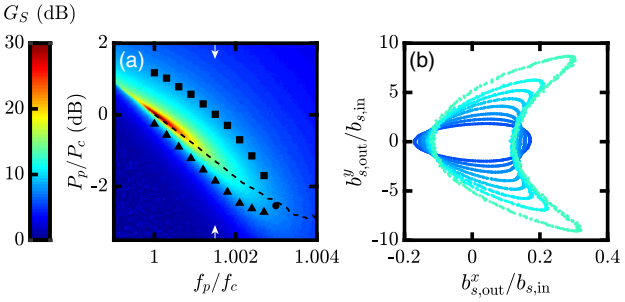

FIG. 3. Dependence of coherent tone distortion upon the amplifier operating point. (a) The SQ gain map, with critical frequency $f_c = 7.0032$ GHz and input critical power $P_c = -93.1$ dBm. (b) Output tone in the IQ plane (input is a circle of unit radius, not shown). The SQ direct gain is varied between 6 (blue) and 13 dB (green) and operated above the LMG at $f_p/f_c = 1.0015$, a frequency indicated by arrows in (a).

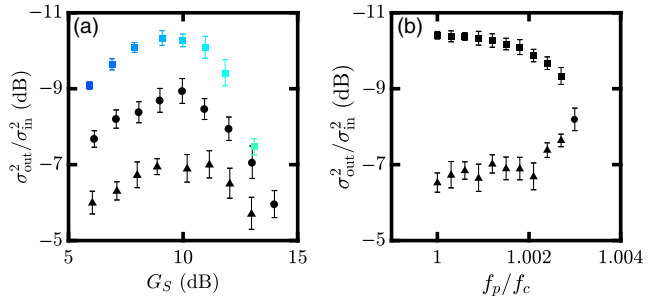

FIG. 4. Dependence of deamplification upon the amplifier operating point. In (a), deamplification is shown as a function of the SQ direct gain when the SQ is operated below (solid triangle) and above (solid square) the LMG (at $f_p/f_c = 1.0015$), as well as on (solid circle) the LMG (where the pump frequency has been varied). In (b), it is shown for the black points in Fig. 3(a), where $G_S = 8$ dB.

relative to below the LMG, visible in Fig. 3(a), we anticipate more linear behavior above the LMG.

To characterize the nonlinear behavior and visualize phasor distortion, we now input a vacuum-sized coherent tone $b_{s,\rm in}e^{i\theta}$ whose phase θ slowly rotates in the SQ pump's frame (Appendix A). With LO and SQ pumps at the same frequency, the tone describes traces at the output in the IQ plane such as those in Fig. 3(b). They are obtained with the SQ operated above the LMG. Thus, by decreasing the pump power, G_S increases from 6 to 13 dB, as the output transitions from ellipse to banana.

Upon repeating the measurement with the SQ off, we characterize deamplification as a function of the SQ operating point by forming the ratio $\sigma^2_{\rm out}/\sigma^2_{\rm in}$, as seen in Sec. II. Figure 4(a) shows these ratios, calculated from the points in Fig. 3(b). Compared to ratios obtained for operating points below and on the LMG for similar sets of JPA gains, we see that the deamplification increases for increasing SQ direct gains less than $G_S = 9$ dB, as the ellipse stretches. Above 9 dB, it decreases due to phasor distortion.

Finally, we study deamplification along a contour of constant direct gain, encircling the critical point, to look for an optimal operating point at which distortion is minimized. Figure 4(b) characterizes the tone's deamplification along the $G_S = 8$ dB contour, at operating points away from bifurcation (i.e., for $f_p > f_c$), indicated in black in Fig. 3(a). Below the LMG $\sigma^2_{\rm out}/\sigma^2_{\rm in}$ is about -7 dB, whereas above it decreases to about -10 dB, as a result of reduced distortion. Thus, operating the SQ above the LMG and with a gain of about 9 dB maximizes deamplification. We leverage these findings in Sec. IV to optimally bias the SQ.

IV. OPTIMIZING VACUUM SQUEEZING

Most applications of microwave squeezed light require the ability to both generate and efficiently detect a squeezed state. We demonstrate these dual capabilities with the AMP, cascaded after the SQ. Upon transport from SQ to AMP, the state suffers from microwave loss η (Fig. 2), which replaces part of the state with an unsqueezed vacuum [38], diminishing the measurable degree of squeezing. We reduce these losses to $\eta = 1.2 \pm 0.2$ dB in our setup (Appendix B) using superconducting cables and a narrow-band triple-junction circulator with an insertion loss < 0.5 dB.

To make a homodyne measurement of vacuum squeezing (see the full setup in Fig. 8, Appendix A), one power generator provides the AMP pump and LO tones, while another, 20 kHz detuned, provides the SQ pump tone. These spectrally adjacent pump tones must be cancelled to avoid AMP saturation and preserve the squeezing of the pure vacuum state generated by our VTS at $T_{\rm VTS} = 55$ mK $\ll \hbar\omega_S/k_B$. We perform these cancellations by combining π-phase-shifted pump tones at the output of each JPA. The AMP acts as a nearly noiseless (Appendix C) phase-sensitive amplifier with roughly 30 dB of single-quadrature gain so as to overwhelm the rest of the amplification chain's added noise. After amplification, the squeezed vacuum is then digitized. A full 2π phase difference θ between the SQ and AMP pumps is swept every $1/20$ kHz $= 50$ μs, and the phase for which the digitized voltage signal is periodically minimized is taken to be the SQ squeezed quadrature. The variance of the voltage fluctuations in this quadrature is thus computed with the SQ on and then again with it off. The reduction in variance when the SQ is on is taken to be the squeezing, $S = \sigma^2_{\rm on}/\sigma^2_{\rm off}$.

We find optimal squeezing occurs at $f_p/f_c = 1.0015$, with direct gain $G_S = 8$ dB, and above the LMG, as expected from Sec. III. Figure 5(a) shows a histogram of

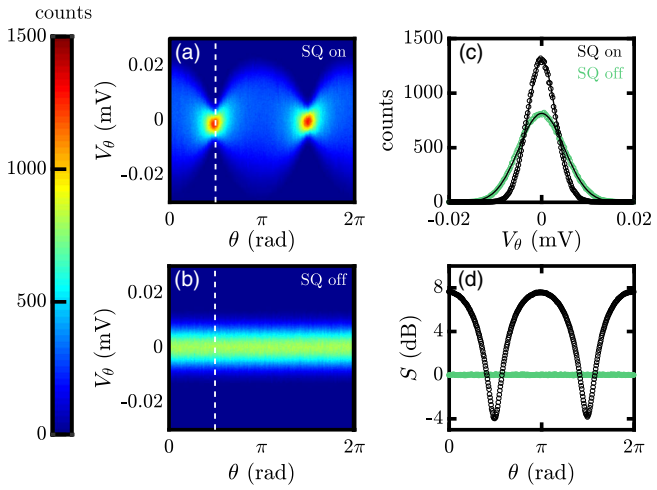

FIG. 5. Vacuum squeezing. The SQ is operated with direct gain $G_S = 8$ dB, obtained with pump frequency $f_p/f_c = 1.0015$ and pump power $P_p/P_c = 0.5045$ dB. (a) Histogram of output voltage fluctuations V_θ along the AMP amplified quadrature with SQ on as a function of the phase difference θ between the SQ and AMP pumps. (b) Histogram with SQ off. (c) Profile of the fluctuations and Gaussian fits (solid lines) along the dashed lines drawn in (a) and (b), at $\theta = \pi/2$. (d) Squeezing $S = \sigma^2_{\rm on}/\sigma^2_{\rm off}$ as a function of θ.

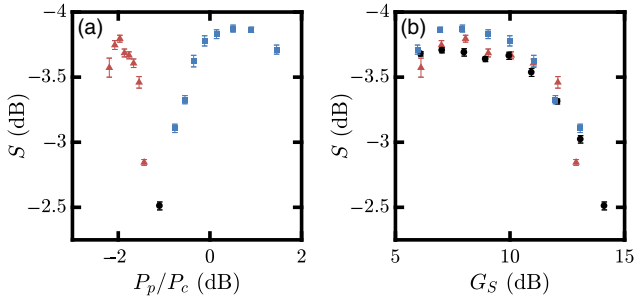

FIG. 6. Dependence of vacuum squeezing on the operating point. (a) The points in red, black, and blue are, respectively, below, on, and above the LMG. Squeezing is plotted as a function of the pump power, for $f_p/f_c = 1.0015$. In (b), it is plotted as a function of the SQ gain, and the red and blue points are those used in (a). For the black points, f_p is varied to obtain gains between 6 and 14 dB.

the voltage fluctuations V_θ retrieved along the AMP amplified quadrature as a function of θ. Compared to Fig. 5(b), where the SQ is off, vacuum is squeezed for $\theta = \pi/2$ and $3\pi/2$. Figure 5(c) presents a cut in the histograms at $\theta = \pi/2$, demonstrating a clear reduction in the Gaussian's standard deviation, and Fig. 5(d) displays the squeezing S as a function of θ, with a minimum of -3.87 ± 0.03 dB. This reduction in the variance, which is measured over a full 30-MHz band centered on the AMP's pump, is not a value inferred at the output of the squeezer but rather one directly measured at the terminus of our measurement chain without any losses or added noises calibrated away.

Moving the SQ operating point, we verify that squeezing decreases as we approach the LMG, due to the increasing gain. Adjusting the pump's power while keeping the frequency constant, we can move the operating point from below to above the LMG, describing a line cut in the gain map, indicated by arrows in Fig. 3(a). Figure 6(a) shows the squeezing along this cut, in qualitative agreement with the theoretical and experimental results on coherent tones seen in Secs. II and III. Furthermore, we obtain a slightly better squeezing above the LMG than below, as expected. This feature is displayed in Fig. 6(b), where squeezing is reported as a function of the SQ gain. As losses are further reduced, we anticipate further improvement in performance, as observed in Sec. III for the deamplification of a coherent tone.

V. CONCLUSION

Pump stiffness is crucial when generating a microwave squeezed state with a JPA, because any deviation from the stiff-pump regime strongly affects the squeezed quadrature. We show that a lack of stiffness distorts output signals, thereby limiting the maximum degree of squeezing. However, we also present a partial solution to this problem by means of choosing the operating point to lie above the LMG, the intuitive choice. Experiments conducted on a coherent tone transformed by a JPA confirm the efficacy of this approach, with less phasor distortion above the LMG. When squeezing a vacuum, we observe the same trend. Maintaining a low microwave loss, we thus generate and deliver a 3.87 ± 0.03 dB vacuum-squeezed state from one JPA to another over a band of 30 MHz.

ACKNOWLEDGMENTS

This work is supported by the National Science Foundation, under Grants No. PHY-1607223 and No. PHY-1734006, and by the Heising-Simons Foundation under Grant No. 2014-183.

APPENDIX A: EXPERIMENTAL SETUP

Our realization of a JPA comprises a TKC (Fig. 7), circulator, and directional coupler. Because the TKC amplifies in reflection, we use a circulator to separate incident and reflected tones, creating input and output ports. It is pumped through the weakly coupled port of a directional coupler [17]. The TKC consists of a series array of $N_s = 20$ SQUIDs with junctions of critical current $I_c = 7$ μA, in parallel with a $C = 550$ fF interdigitated capacitor. This lumped element resonator connects through a coupling capacitance $C_c = 70$ fF to a coplanar waveguide. The TKC has bare resonant frequency $f_0 = 7.3$ GHz and quality factor $Q = 65$.

The full experimental setup is represented in Fig. 8. SQ and AMP TKCs are individually magnetically shielded. They can be tuned via coils biased by current sources. The generator which provides the AMP pump and cancellation tones also sources the LO. A switch may be used to turn off the AMP pump without interrupting the LO. A third generator (far left in Fig. 8) is used to create the probe tone. Output signals are demodulated with an IQ mixer and then digitized. A vector network analyzer (VNA) is used to determine the direct gains, and a spectrum analyzer (SA)

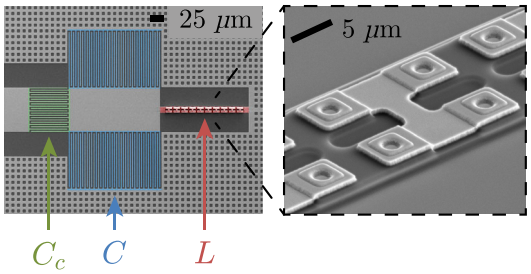

FIG. 7. Scanning-electron-microscope images of a TKC. The chip is fabricated in a niobium-aluminum-niobium trilayer process. The waffling pattern covering the niobium ground plane pins the magnetic flux trapped in the superconductor in place. A close-up view of part of the SQUID array shows four Josephson junctions, located at the ends of the bright H shape. With the base niobium electrode (dark gray), they form two SQUID loops.

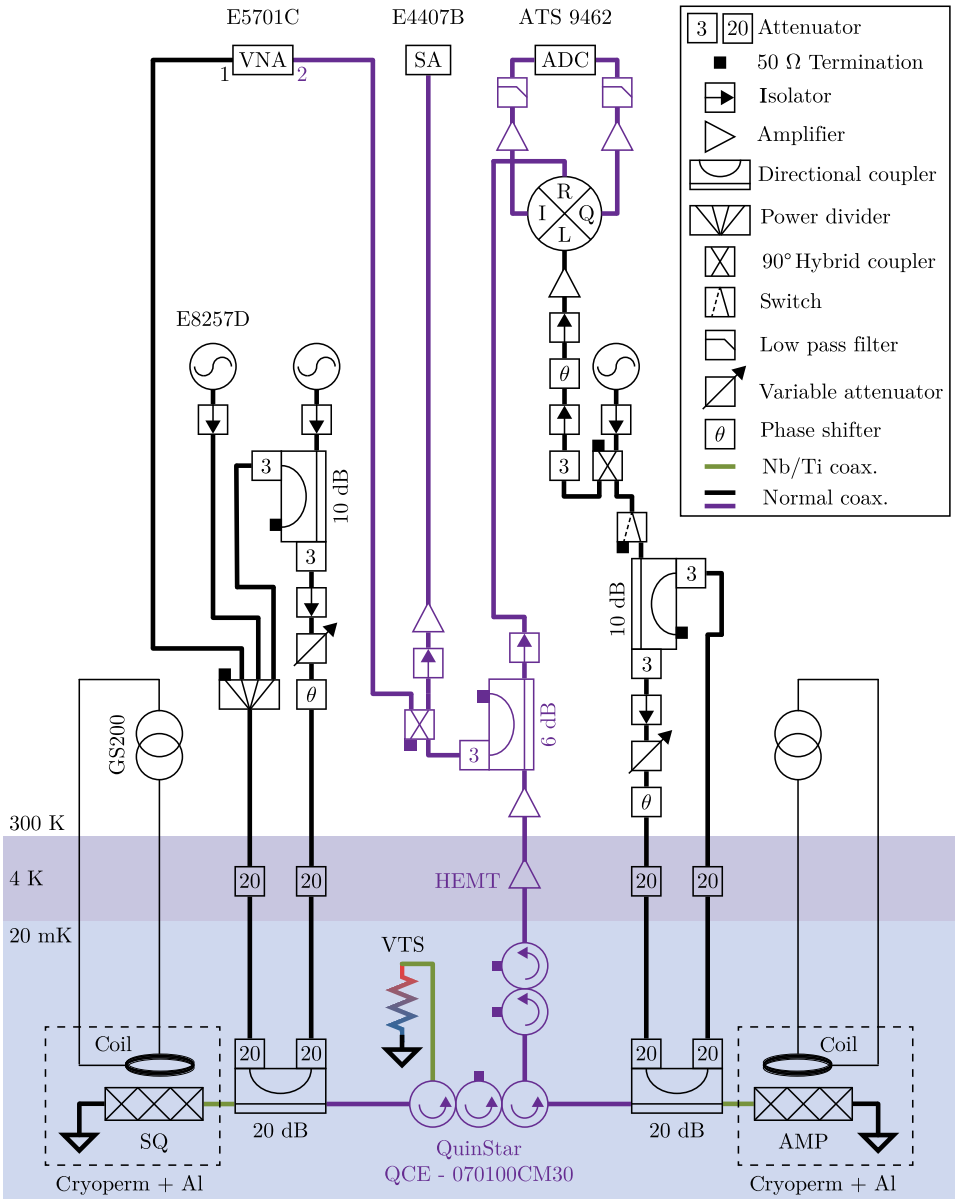

FIG. 8. Full experimental setup used for both coherent tone deamplification and squeezing. The input and output coaxial cables are colored in black and purple, respectively. The green lines are superconducting.

monitors pump cancellation. Each cancel line consists of a variable attenuator and a phase shifter. Several isolators and 3-dB attenuators are placed in the setup to minimize harmful reflections.

At base temperature, a triple-junction circulator links the SQ and AMP TKCs. It provides > 50 dB isolation between the SQ and AMP and has a low insertion loss (< 0.5 dB). A VTS, weakly coupled to the base temperature plate and composed of a 50 Ω load, a heater, and a thermometer, generates the chain's input noise and allows for the measurement of SQ-added noise. Superconducting Nb/Ti lines are placed between TKCs and DCs to further reduce microwave loss, and the DCs are directly connected to the circulator with swept elbows.

To measure the distortion of a coherent tone (Sec. III), we adjust its power to $P_{\mathrm{PR}} = \frac{1}{2}\hbar\omega B$ in order to keep it comparable to the vacuum, with B the SQ bandwidth. With the LO generator at the same frequency as the SQ pump, we detune the tone by $f_{\mathrm{PR}} - f_p = 20$ kHz, so that its phasor slowly rotates in the LO's frame, enabling the measurement of 360 independent phasors within the 15-MHz IF bandwidth of our readout chain. Because of the feeble input signal, we heavily average the two output quadratures, which then describe traces in the IQ plane such as those in Fig. 3(b).

APPENDIX B: LINE CALIBRATION

Calibrating the lines relies on measuring the overall input attenuation A^I from the probe tone's microwave generator to the SQ input and also the overall amplifications G_A^O and G_S^O from the TKC outputs to the analog-to-digital converter (ADC). Knowing A^I allows for the calibration of the probe power incident on the SQ TKC, and the ratio $\eta = G_A^O/G_S^O$

provides, *ceteris paribus*, an estimate of the loss experienced by the squeezed state when traveling between the SQ and AMP.

Operating one JPA at a time (without pump cancellation), G_A^O and G_S^O are calculated by integrating the power spectral density of vacuum fluctuations recorded by the ADC over a window $W = 500$ kHz within the JPA's bandwidth. To avoid dc offsets, we perform a heterodyne measurement, with the LO and JPA pump detuned by 5 MHz and W ending 400 kHz below the pump. Thus, when measuring G_A^O, the generator used for pumping is the one connected to the SQ, itself detuned. The SQ TKC then simply acts as a mirror, and the pump tone reaches the AMP after reflection. Given a quantum at the SQ or AMP input, the integrated power for both cases is

$$P_{A/S}^O = \hbar\omega W G_{A/S}^O G_{A/S}, \tag{B1}$$

with $G_{A/S}$ the AMP or SQ gain, measured with the VNA. We operate the JPAs at various gains between 20 and 30 dB, ensuring that the output spectral density linearly tracks the JPA gain, and obtain

$$\begin{aligned} \text{AMP to ADC} \quad & G_A^O = 76.5 \pm 0.1 \text{ dB}, \\ \text{SQ to ADC} \quad & G_S^O = 75.3 \pm 0.1 \text{ dB}. \end{aligned}$$

Therefore, we estimate that $\eta = 1.2 \pm 0.2$ dB. In principle, this value should enable us to observe about 5.6 dB of squeezing, a bit more than what we measured. But in practice, we are limited by a combination of squeezed state distortion and the contribution from the HEMT added noise, which becomes harder to overwhelm when squeezing.

We estimate A^I with a similar protocol. Turning off both JPAs, a probe tone with input power P_P^I traveling in the lines creates an output power P_P^O on the ADC as

$$P_P^O = P_P^I G_S^O A^I. \tag{B2}$$

We thus estimate $A^I = -81.4 \pm 0.2$ dB.

APPENDIX C: SQ ADDED NOISE

Any resistor at temperature T generates noise of a known variance, whose spectral density in units of quanta at angular frequency ω is

$$S_{\text{in}} = \frac{1}{2} + \frac{1}{e^{\hbar\omega/k_B T} - 1}. \tag{C1}$$

Our VTS therefore allows us to generate a known thermal state at the chain's input, which is then amplified by the SQ, giving at its output:

$$S_{S,\text{out}} = G_S(S_{\text{in}} + N_S), \tag{C2}$$

where G_S is the SQ gain and N_S its added noise (in this experiment, we use only the SQ; the AMP is detuned). Since we are operating the SQ in a phase-sensitive mode, $N_S \geq 0$.

In practice, there are inefficiencies in the thermal state's transportation from VTS to SQ. We can model these with a simple beam-splitter picture, such that a fraction λ of S_{in} is replaced with noise S_f at the fridge's temperature. Considering the system-added noise as $N_{\text{add}} = N_S + N_H/G_S$, where N_H is the HEMT-added noise, we have

$$\begin{aligned} S_{\text{out}} &= G_S^O G_S[\lambda S_{\text{in}} + (1-\lambda)S_f + N_{\text{add}}] \\ &= G_S^O G_S S_{\text{out}}^{\text{in}} \end{aligned} \tag{C3}$$

at the output of the chain, where G_S^O is the chain's gain and $S_{\text{out}}^{\text{in}}$ is the output noise spectral density referred to the SQ input. Varying S_{in} and S_f, we thus can deduce N_{add} and λ.

With a homodyne configuration (LO and SQ pump at the same frequency), we integrate the output noise spectral density S_{out} over the SQ bandwidth B for various VTS temperatures. The fridge's base temperature T_f is fixed, and $G_S \geq 25$ dB is tracked by amplifying and measuring a small pilot tone. Figure 9 shows $S_{\text{out}}^{\text{in}}$ as a function of the VTS temperature for three different fridge temperatures. A fit gives $N_{\text{add}} = 0.045 \pm 0.001$ and $\lambda = 0.79 \pm 0.01$, where the quoted uncertainties correspond to statistical errors in the measurements.

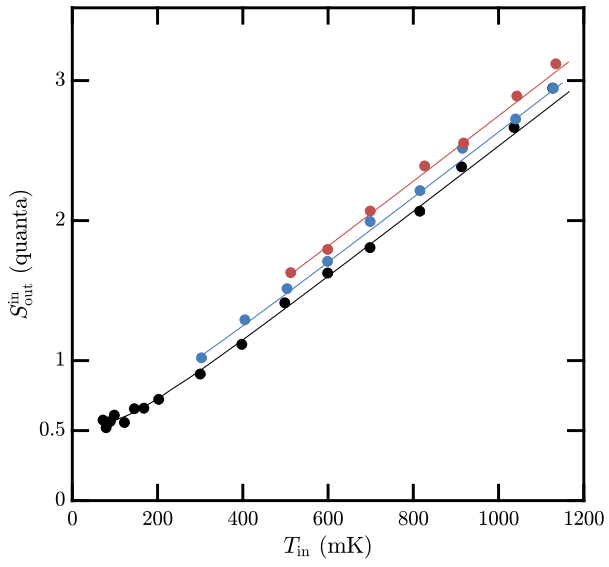

FIG. 9. Noise spectral density as a function of the VTS temperature. The noise is referred to the SQ input. Points in black, blue, and red are for fridge temperatures $T_f = 50$, 300, and 500 mK, respectively. The statistical error is smaller than the point size. The solid lines are obtained from fitting the parameters N_{add}, λ, and the overall gain of the chain $G_S^O G_S$.

[1] R. Vijay, D. H. Slichter, and I. Siddiqi, Observation of Quantum Jumps in a Superconducting Artificial Atom, Phys. Rev. Lett. **106**, 110502 (2011).
[2] Z. R. Lin, K. Inomata, W. D. Oliver, K. Koshino, Y. Nakamura, J. S. Tsai, and T. Yamamoto, Single-shot readout of a superconducting flux qubit with a flux-driven Josephson parametric amplifier, Appl. Phys. Lett. **103**, 132602 (2013).
[3] M. Hatridge, S. Shankar, M. Mirrahimi, F. Schackert, K. Geerlings, T. Brecht, K. M. Sliwa, B. Abdo, L. Frunzio, S. M. Girvin, R. J. Schoelkopf, and M. H. Devoret, Quantum back-action of an individual variable-strength measurement, Science **339**, 178 (2013).
[4] D. Ristè, J. G. van Leeuwen, H.-S. Ku, K. W. Lehnert, and L. DiCarlo, Initialization by Measurement of a Superconducting Quantum Bit Circuit, Phys. Rev. Lett. **109**, 050507 (2012).
[5] William F. Kindel, M. D. Schroer, and K. W. Lehnert, Generation and efficient measurement of single photons from fixed-frequency superconducting qubits, Phys. Rev. A **93**, 033817 (2016).
[6] K. W. Murch, S. J. Weber, K. M. Beck, Eran Ginossar, and I. Siddiqi, Reduction of the radiative decay of atomic coherence in squeezed vacuum, Nature (London) **499**, 62 (2013).
[7] Sh. Barzanjeh, D. P. DiVincenzo, and B. M. Terhal, Dispersive qubit measurement by interferometry with parametric amplifiers, Phys. Rev. B **90**, 134515 (2014).
[8] Nicolas Didier, Archana Kamal, William D. Oliver, Alexandre Blais, and Aashish A. Clerk, Heisenberg-Limited Qubit Readout with Two-Mode Squeezed Light, Phys. Rev. Lett. **115**, 093604 (2015).
[9] Nicolas Didier, Jérôme Bourassa, and Alexandre Blais, Fast Quantum Nondemolition Readout by Parametric Modulation of Longitudinal Qubit-Oscillator Interaction, Phys. Rev. Lett. **115**, 203601 (2015).
[10] Jeremy B. Clark, Florent Lecocq, Raymond W. Simmonds, José Aumentado, and John D. Teufel, Observation of strong radiation pressure forces from squeezed light on a mechanical oscillator, Nat. Phys. **12**, 683 (2016).
[11] A. Bienfait, P. Campagne-Ibarcq, A. H. Kiilerich, X. Zhou, S. Probst, J. J. Pla, T. Schenkel, D. Vion, D. Esteve, J. J. L. Morton, K. Moelmer, and P. Bertet, Magnetic Resonance with Squeezed Microwaves, Phys. Rev. X **7**, 041011 (2017).
[12] P. Sikivie, Experimental Tests of the "Invisible" Axion, Phys. Rev. Lett. **51**, 1415 (1983).
[13] Huaixiu Zheng, Matti Silveri, R. T. Brierley, S. M. Girvin, and K. W. Lehnert, Accelerating dark-matter axion searches with quantum measurement technology, arXiv:1607.02529.
[14] B. M. Brubaker, L. Zhong, Y. V. Gurevich, S. B. Cahn, S. K. Lamoreaux, M. Simanovskaia, J. R. Root, S. M. Lewis, S. Al Kenany, K. M. Backes, I. Urdinaran, N. M. Rapidis, T. M. Shokair, K. A. van Bibber, D. A. Palken, M. Malnou, W. F. Kindel, M. A. Anil, K. W. Lehnert, and G. Carosi, First Results from a Microwave Cavity Axion Search at 24 μeV, Phys. Rev. Lett. **118**, 061302 (2017).
[15] S. Al Kenany, M. A. Anil, K. M. Backes, B. M. Brubaker, S. B. Cahn, G. Carosi, Y. V. Gurevich, W. F. Kindel, S. K. Lamoreaux, K. W. Lehnert, S. M. Lewis, M. Malnou, D. A. Palken, N. M. Rapidis, J. R. Root, M. Simanovskaia, T. M. Shokair, I. Urdinaran, K. A. van Bibber, and L. Zhong, Design and operational experience of a microwave cavity axion detector for the 20-100ev range, Nucl. Instrum. Methods Phys. Res., Sect. A **854**, 11 (2017).
[16] M. A. Castellanos-Beltran, K. D. Irwin, G. C. Hilton, L. R. Vale, and K. W. Lehnert, Amplification and squeezing of quantum noise with a tunable Josephson metamaterial, Nat. Phys. **4**, 929 (2008).
[17] F. Mallet, M. A. Castellanos-Beltran, H. S. Ku, S. Glancy, E. Knill, K. D. Irwin, G. C. Hilton, L. R. Vale, and K. W. Lehnert, Quantum State Tomography of an Itinerant Squeezed Microwave Field, Phys. Rev. Lett. **106**, 220502 (2011).
[18] E. P. Menzel, R. Di Candia, F. Deppe, P. Eder, L. Zhong, M. Ihmig, M. Haeberlein, A. Baust, E. Hoffmann, D. Ballester, K. Inomata, T. Yamamoto, Y. Nakamura, E. Solano, A. Marx, and R. Gross, Path Entanglement of Continuous-Variable Quantum Microwaves, Phys. Rev. Lett. **109**, 250502 (2012).
[19] Samuel Boutin, David M. Toyli, Aditya V. Venkatramani, Andrew W. Eddins, Irfan Siddiqi, and Alexandre Blais, Effect of Higher-Order Nonlinearities on Amplification and Squeezing in Josephson Parametric Amplifiers, Phys. Rev. Applied **8**, 054030 (2017).
[20] G. Liu, T.-C. Chien, X. Cao, O. Lanes, E. Alpern, D. Pekker, and M. Hatridge, Josephson parametric converter saturation and higher order effects, Appl. Phys. Lett. **111**, 202603 (2017).
[21] K. M. Sliwa, M. Hatridge, A. Narla, S. Shankar, L. Frunzio, R. J. Schoelkopf, and M. H. Devoret, Reconfigurable Josephson Circulator/Directional Amplifier, Phys. Rev. X **5**, 041020 (2015).
[22] Joseph Kerckhoff, Kevin Lalumière, Benjamin J. Chapman, Alexandre Blais, and K. W. Lehnert, On-Chip Superconducting Microwave Circulator from Synthetic Rotation, Phys. Rev. Applied **4**, 034002 (2015).
[23] F. Lecocq, L. Ranzani, G. A. Peterson, K. Cicak, R. W. Simmonds, J. D. Teufel, and J. Aumentado, Nonreciprocal Microwave Signal Processing with a Field-Programmable Josephson Amplifier, Phys. Rev. Applied **7**, 024028 (2017).
[24] A. C. Mahoney, J. I. Colless, S. J. Pauka, J. M. Hornibrook, J. D. Watson, G. C. Gardner, M. J. Manfra, A. C. Doherty, and D. J. Reilly, On-Chip Microwave Quantum Hall Circulator, Phys. Rev. X **7**, 011007 (2017).
[25] Benjamin J. Chapman, Eric I. Rosenthal, Joseph Kerckhoff, Bradley A. Moores, Leila R. Vale, J. A. B. Mates, Gene C. Hilton, Kevin Lalumière, Alexandre Blais, and K. W. Lehnert, Widely Tunable On-Chip Microwave Circulator for Superconducting Quantum Circuits, Phys. Rev. X **7**, 041043 (2017).
[26] T. Yamamoto, K. Inomata, M. Watanabe, K. Matsuba, T. Miyazaki, W. D. Oliver, Y. Nakamura, and J. S. Tsai, Flux-driven Josephson parametric amplifier, Appl. Phys. Lett. **93**, 042510 (2008).
[27] L. Zhong, E. P. Menzel, R. Di Candia, P. Eder, M. Ihmig, A. Baust, M. Haeberlein, E. Hoffmann, K. Inomata, T. Yamamoto, Y. Nakamura, E. Solano, F. Deppe, A. Marx, and R. Gross, Squeezing with a flux-driven Josephson parametric amplifier, New J. Phys. **15**, 125013 (2013).
[28] X. Zhou, V. Schmitt, P. Bertet, D. Vion, W. Wustmann, V. Shumeiko, and D. Esteve, High-gain weakly nonlinear

flux-modulated Josephson parametric amplifier using a squid array, Phys. Rev. B **89**, 214517 (2014).

[29] Stefan Pogorzalek, Kirill G. Fedorov, Ling Zhong, Jan Goetz, Friedrich Wulschner, Michael Fischer, Peter Eder, Edwar Xie, Kunihiro Inomata, Tsuyoshi Yamamoto, Yasunobu Nakamura, Achim Marx, Frank Deppe, and Rudolf Gross, Hysteretic Flux Response and Nondegenerate Gain of Flux-Driven Josephson Parametric Amplifiers, Phys. Rev. Applied **8**, 024012 (2017).

[30] C. Macklin, K. O'Brien, D. Hover, M. E. Schwartz, V. Bolkhovsky, X. Zhang, W. D. Oliver, and I. Siddiqi, A near–quantum-limited Josephson traveling-wave parametric amplifier, Science **350**, 307 (2015).

[31] M. A. Castellanos-Beltran and K. W. Lehnert, Widely tunable parametric amplifier based on a superconducting quantum interference device array resonator, Appl. Phys. Lett. **91**, 083509 (2007).

[32] V. E. Manucharyan, E. Boaknin, M. Metcalfe, R. Vijay, I. Siddiqi, and M. H. Devoret, Microwave bifurcation of a Josephson junction: Embedding-circuit requirements, Phys. Rev. B **76**, 014524 (2007).

[33] Archana Kamal, Adam Marblestone, and M. H. Devoret, Signal-to-pump back action and self-oscillation in double-pump Josephson parametric amplifier, Phys. Rev. B **79**, 184301 (2009).

[34] C. W. Gardiner and M. J. Collett, Input and output in damped quantum systems: Quantum stochastic differential equations and the master equation, Phys. Rev. A **31**, 3761 (1985).

[35] B. Yurke and E. Buks, Performance of cavity-parametric amplifiers, employing Kerr nonlinearities, in the presence of two-photon loss, J. Lightwave Technol. **24**, 5054 (2006).

[36] K. V. Kheruntsyan, Wigner function for a driven anharmonic oscillator, J. Opt. B **1**, 225 (1999).

[37] B. Yurke, L. R. Corruccini, P. G. Kaminsky, L. W. Rupp, A. D. Smith, A. H. Silver, R. W. Simon, and E. A. Whittaker, Observation of parametric amplification and deamplification in a Josephson parametric amplifier, Phys. Rev. A **39**, 2519 (1989).

[38] U. Leonhardt and H. Paul, Measuring the quantum state of light, Prog. Quantum Electron. **19**, 89 (1995).